Environmental Research 202 (2021) 111707

Contents lists available at ScienceDirect

Environmental Research

journal homepage: www.elsevier.com/locate/envres

Quercetin-rGO based mercury-free electrode for the determination of toxic Cd (II) and Pb (II) ions using DPASV technique

K. Krishna Kumar [a,c], M. Devendiran [b], P. Senthil Kumar [c,d,*], S. Sriman Narayanan [a,**]

[a] Department of Analytical Chemistry, School of Chemical Science, University of Madras, Guindy Campus, Chennai, Tamil Nadu, 600025, India
[b] Central Instrumentation Laboratory, Vels Institute of Science Technology and Advanced Studies, Pallavaram, Chennai, Tamil Nadu, 600025, India
[c] Department of Chemical Engineering, Sri Sivasubramaniya Nadar College of Engineering, Chennai, 603110, India
[d] Centre of Excellence in Water Research (CEWAR), Sri Sivasubramaniya Nadar College of Engineering, Chennai, 603110, India

ARTICLE INFO

Keywords:
Quercetin
Reduced graphene oxide
Chemically modified electrode
Metal ions
Stripping voltammetry

ABSTRACT

Metal ion pollution poses serious threat to environment. Analysis of Cd (II) and Pb (II) ions using chemically modified mercury free electrode is a feasible routine analytical tool. Developing an electrode surface modified with conductive 2D carbon and metal complexing ligand created a synergetic effect towards sensitive and selective electrochemical determination of metal ions. The present study focused on green chemistry approach towards synthesis of reduced graphene oxide using a natural flavonoid (Quercetin) that acts as a reducing, functionalizing agent and also as metal complexing agent. This quercetin reduced graphene oxide (Q-rGO) was surface modified over paraffin wax impregnated graphite electrode. The resulting Q-rGO electrode was used as a mercury-free electrode for simultaneous analysis of Pb (II) and Cd (II) ions. Physico-chemical parameters of the synthesized Q-rGO and modified electrodes were characterized using X-ray diffraction, UV–Vis, FT-IR, and Raman spectrometer. The morphology of the material and surface topography of the modified electrode was observed using HR-TEM and FESEM, respectively. Cyclic voltammetry (CV) and AC impedance (EIS) were adopted for electrochemical characterization and Differential pulse anodic stripping voltammetry (DPASV) was chosen for simultaneous sensing of metal ions using Q-rGO electrode. Analytical parameters such as effect of electrolyte, effect of pH, preconcentration time and deposition potential were optimized. The experimental results suggested that the Q-rGO electrode is capable of sensing Pb (II) and Cd (II) ions individually and simultaneously. Inference from the calibration plot showed that the Q-rGO electrode was capable of sensing the concentration range of Cd (II) ion form 0.19 to 2.5 μgL^{-1} with LOD-0.05 μgL^{-1} and Pb (II) ions from 0.19 to 3.1 μgL^{-1} with LOD 0.06 μgL^{-1}.

1. Introduction

The human population is seriously threatened by environmentally hazardous inorganic heavy metal pollutant such as Hg (II), Pb (II), Cd (II), Zn (II), Cu (II) etc [Sriram, G, 2017]. High level contaminations of these pollutants are prevalent in the water system due to industrialization and life style. Some of the above mentioned pollutant contributes for the fatal diseases such as Cancer, Parkinson's etc [Kilaru HarshaVardhan, 2019]. Occurrence of these diseases is common in metropolitan areas as well as in the rural areas. Hence it is important for the periodic monitoring of these pollutants. Several analytical methods, protocols and standard procedures have been established for the quantitative and qualitative estimation of aforementioned pollutants. Among them ion-exchange chromatography [Sarzanini, C, 2001], spectroscopy [Khalid Siraj, 2013], and inductively coupled plasma resonance methods [K.A. Isai 2015] have been widely used analytical techniques in industries and research. Although these techniques are accepted by several regulatory bodies, periodic monitoring of these pollutant are hardly possible due to sophisticated instrumentation, tedious sample preparation, and in-house analysis [Lu, Y, 2018]. Electroanalytical methods overcomes the limitation of other techniques with miniaturized cost effective instruments, field analysis, low sample volume, simple

* Corresponding author. Centre of Excellence in Water Research (CEWAR), Sri Sivasubramaniya Nadar College of Engineering, Rajiv Gandhi Salai, Kalavakkam, 603 110. Tamilnadu, India.
** Corresponding author. Department of Analytical Chemistry, School of Chemical Sciences, University of Madras, Guindy Campus, Chennai, 600025, Tamil Nadu, India.
E-mail addresses: senthilkumarp@ssn.edu.in, senthilchem8582@gmail.com (P. Senthil Kumar), sriman55@yahoo.com (S. Sriman Narayanan).

https://doi.org/10.1016/j.envres.2021.111707
Received 31 May 2021; Received in revised form 10 July 2021; Accepted 13 July 2021
Available online 16 July 2021

method of analysis, direct sensing with no pre-sampling procedures, and picomolar sensing of analysts [[a]Hassan Karimi-Maleh, 2021] [[b]Hassan Karimi-Maleh, 2021]. Simultaneous analysis of individual and multiple analytes without overlapping or interference can be achieved using electroanalytical methods [Tahernejad-Javazmi, 2018]. By Differential Pulse Anodic Stripping Voltammetry (DPASV) technique, heavy metal pollutants can be specifically analyzed with preconcentration, pre-anodisation and stripping procedures [Lu, Y, 2018]. Conventionally, mercury based electrodes were employed for metal ion sensing, but again the toxicity associated with mercury seeks an alternate electrode for stripping voltammetric analysis of metal ions. There are several chemically modified electrodes (CMEs) developed as an alternate to mercury based electrodes towards determination of toxic metal ions. But the present work described about the synergetic effect of composite material consisting of natural chelating ligand (Quercetin) and a conducting 2D carbon based material (rGO). Fabricating the electrode surface with such composite enhanced the electrochemical performance with good sensitivity [Tahernejad-Javazmi, 2019], [Hassan Karimi-Maleh, 2020]. Functionalized biopolymer is found to be suitable electrode material for adsorption preconcentration of Pb (II) ions [Anitha, T, 2015].

Graphene, a 2-dimensional monolayer, honeycomb crystal lattice of carbon atoms and it is the basic building block of all graphitic materials [A.K. Geim, 2007]. Single layered graphene sheets were first isolated from graphite flakes using the scotch tape method by Novoselov and Geim in 2004 [K. S. Novoselov, 2004]. The graphene possesses superior electrical [K. S. Novoselov, 2005], electrochromic [B. Gadgil, 2015], mechanical [C. Lee, 2016] and thermal properties [A.A. Balandin, 2008], The unique 2D structure of graphene increased its attention in various fields from optical instruments, solar cells, sensors, thin-film transistors and photocatalysis, biosensor [G. Gnana Kumar, 2014] [Mohanraj, J, 2020]. Versatile application of 2D carbon increased the demand for the large scale production of graphene. Conventional techniques used for high quality and high yield of graphene are by physical and chemical methods. The term 'graphene' is used for the monolayer/few layers of graphene sheets prepared by bottom-up approach/physical method [B. Gadgil, 2015]. On the other hand when graphene is prepared by the top-down approach/chemical methods, usually by the reduction of graphite oxide, the resulting material is termed as 'reduced graphene oxide' (rGO) [Y.F.X. Wang, 2014]. Chemical reduction of graphite oxide into rGO is usually done with the help of poisonous reductant. In the chemical reduction process, the oxygen containing functional groups of graphene oxide (GO) such as carboxyl, hydroxyl and epoxy groups are reduced with the help of these reducing agents resulting in the formation of rGO with more C–C bonds. Although the chemical methods can result in higher yields of rGO than physical methods, toxicity associated with the usage of reducing agents is one of the major environmental concerns [Y.N. Singhbabu, 2013]. Moreover, it is highly difficult to remove the impurities produced by these reducing agents [C. Singh, 2016]. Therefore, environment friendly and non-toxic reducing agents are need of the hour for the production of rGO.

For the past few years, green chemistry has contributed many non-toxic innovative methods for the reduction of graphite oxide into rGO. Various agents such as phytochemicals of *Azadirachta indica* extract [G. Gnana Kumar, 2014], fenugreek extract [C. Singh, 2016], *Terminalia bellerica* extract [S.B. Maddinedi, 2016], *Annona squamosa* extract [B. Chandu, 2017], caffeic acid [Z. Bo, 2014], green tea extract [Y. Wang, 2011], glucose [I. Akin, 2014] etc, have been used for green synthesis of rGO. Apart from reducing the GO sheets, these agents are also capable of providing unique functional groups and properties for the rGO sheets. The reviews [S. Thakur, 2015] [M. T. H. Aunkor, 2016] listed the existing literature reporting the green reduction of GO using natural reagents. Plant polyphenols such as curcumin is one such material for the effective reduction of GO to rGO and several studies using curcumin for the reduction and functionalization of GO have been reported for cancer treatment [S. Hatamie, 2015]. Another closely related flavonoid molecule to curcumin is quercetin which is also found to possess reducing capacity.

Quercetin, chemically known as 3, 5, 7, 3′, 4′-pentahydroxyflavone is a natural flavonoid obtained from many vegetable and fruit extracts. It was well known for its various applications ranging from electrochemical analysis to nanoparticles synthesis. Quercetin is found to possess electrocatalytic activity which makes them a suitable mediator for the fabrication of chemically modified electrodes (CMEs) [Z. Wang, 2011]. It also exhibits strong chelating activity with many metal ions due to the presence of carbonyl, hydroxyl group at C3 and C5 position and catechol group of C3′ and C4' [B.A. Zsembik, 2006]. Quercetin has been used as a capping and reducing agent for the green synthesis of gold nanoparticles [R.M. Devendiran, 2016]. It is also found to be a suitable analytical reagent for the voltametric determination of Antimony (III) [C. Rojas, 2013].

Although quercetin exhibits such versatile and desirable properties, there is no existing report where quercetin was employed as functionalizing and reducing agent during synthesis of rGO. In this study, we have successfully prepared rGO using quercetin as a reducing, stabilizing and functionalizing agent. Quercetin reduced graphene oxide (Q-rGO) was fabricated onto the paraffin wax impregnated graphite (PIG) electrode surface and used as a mercury-free electrode for the determination of metal ions. Previous study stated that the application of sulfonated biomaterials for adsorption and removal of Pb (II) ions [A. Saravanan, 2021][a], Cd (II) ions [A. Saravanan, 2021][b], and Cr (VI) ions [S. Suganya, 2018] pollutant from water system. Similarly quercetin also has the property to form metal complex. The presence of biomaterial quercetin at the surface of the rGO sheets exhibits redox property and also acts as metal chelating ligand by complexing with lead and cadmium ions. Owing to this property, the Q-rGO electrode was employed for the analysis of Cd (II) and Pb (II) ions using DPASV technique.

2. Methodology

2.1. Materials, chemicals and reagents

Graphite powder, a spectroscopic grade graphite rod (Length- 150 mm, Diameter- 3 mm), the analytical standards of cadmium acetate and lead acetate were procured from Sigma-Aldrich and quercetin was obtained from SRL Chemicals. All other chemicals used in this study such as ammonium sulfate ($(NH_4)_2SO_4$), acetic acid, ammonium nitrate (NH_4NO_3), dipotassium hydrogen phosphate (K_2HPO_4), hydrogen peroxide (30% H_2O_2), potassium sulfate (K_2SO_4), potassium permanganate ($KMnO_4$), potassium nitrate (KNO_3), potassium dihydrogen phosphate (KH_2PO_4), sodium acetate (CH_3COONa), sulphuric acid (H_2SO_4) sodium sulfate (Na_2SO4), and sodium nitrate ($NaNO_3$), were procured from Merck. All the aqueous reagents and buffers were prepared using double distilled (DD) water.

2.2. Instrumentation

Material characterizations of synthesized GO and Q-rGO was done using UV–Visible absorption spectroscopy, recorded in Diode array spectrophotometer, model-8453 (Agilent technologies, USA), Powder XRD spectra obtained with Bruker D8 advance X-Ray Diffraction (Cu Kα radiation) and the morphology of Q-rGO was obtained using High Resolution Transmitted Electron Microscopic (HR-TEM) imaging and selected area electron diffraction (SAED) pattern were performed with H7650 Microscope (Hitachi, Japan).

For the surface characterization of unmodified PIG and modified working electrodes, the IR spectra were recorded using Fourier Transform Infra-Red (FTIR) spectrometer, model- Cary 630 (Agilent technologies, USA) in Attenuated Total Reflection (ATR) mode and Raman spectra were recorded using 532 nm laser beam Raman 11i system

(Nanophoton Corp., Japan). The morphology of the electrodes was analyzed using Field Emission Scanning Electron Microscope (FESEM) model- Quanta FEG 200 (FEI, USA). All the electrochemical analysis such as CV, EIS, Chronoamperomerty, DPASV were performed using electrochemical workstation, model- 660 B (CH Instruments, USA) in a three-electrode cell setup, (i) reference electrode-standard calomel electrode, (ii) auxiliary/counter electrode-platinum electrode and (iii) working electrode-CMEs. In this study, four CMEs were chosen as working electrode for comparison such as (a) unmodified PIG, (b) graphene oxide (GO), (c) quercetin (Q) and (d) quercetin-reduced graphene oxide (Q-rGO) electrodes. The solutions pH and buffers were make-up using ELICO pH meter (Model CM-180).

2.3. Synthesis of GO

Graphene oxide (GO) was prepared by modified Hummer's method [William S. Hummers, 1958]. Briefly, 2 g of graphite fine powder and 1 g of $NaNO_3$ were mixed with 100 ml of conc. H_2SO_4 for 30 min under an ice bath (<10 °C). Following this, $KMnO_4$ (7 g) was added in little portions to prevent any explosion. After addition of $KMnO_4$, the color change from black powder to purple slurry was observed. The slurry was left to stir under an ice bath for 1 h. The slurry mixture was removed from the ice bath and stirred continuously for 24 h for efficient oxidation resulting in dark brown color. To this, DD water (100 ml) was added very slowly which caused an exothermic reaction. After the heat subsided, DD water (500 ml) was added in excess. To stop the reaction, add 10 ml of H_2O_2 (30%) solution which resulted in bright yellow-orange colored suspension. Keep it undisturbed for overnight and discard the supernatant. Filter the resulting precipitate and washed with 10% HCl several times to remove impurities. Finally neutralized the resulting mixture by washing with DD water and GO slurry was obtained by centrifugation. The slurry was vacuum dried in the oven resulting in graphite oxide flakes and sonication of graphite oxide in DD water resulted in well dispersed Graphene Oxide (GO).

2.4. Green synthesis of Q-rGO

Chemically exfoliated GO was simultaneously reduced and functionalized using quercetin by following the procedure previously reported for the synthesis of curcumin reduced and functionalized rGO composite [S. Hatamie, 2015]. Briefly, to the prepared GO suspension, 10 ml of an ethanolic solution containing 5 mg of quercetin was added under stirring. To facilitate the reduction of GO to rGO, pH of the medium was raised to pH 10 with the addition of 10 μL ammonia solution and increased the temperature to 85 °C for 30 min under stirring. The change in color from brown to black indicates the successful reduction of GO to rGO. Finally, the quercetin functionalized reduced graphene oxide (Q-rGO) was neutralized with DD water and centrifuged at 3500 rpm to obtain the material.

2.5. Electrode preparation

The graphite electrode was impregnated with paraffin wax as reported previously [F. Scholz, 1992] under vacuum to block the pores present at the sidewall of the rod. The PIG electrode was surface polished with 350 μm followed by 1000 μm emery paper. The surface of the electrode was smoothed to a mirror finish by polishing on different alumina slurry of 0.1, 0.3, and 0.05 μm size and washed with DD water. CMEs were prepared by 5 μL of drop-casting GO, quercetin and Q-rGO to individual unmodified PIG electrode surface. These CMEs were used as the working electrodes for comparative study during analysis.

3. Results and discussion

3.1. Characterization of physico-chemical properties

The physico-chemical characteristics of synthesized material were studied using spectroscopic and microscopic techniques. The crystalline property of graphite, quercetin, GO and Q-rGO, were studied using XRD analysis and the results are shown in Fig. 1(i). The diffraction pattern (a) corresponds to the pristine graphite which showed a sharp peak (0 0 2) at $2\theta = 26.65^\circ$ with an interlayer d spacing of 0.33 nm. The diffraction pattern (b) for quercetin showed multiple peaks confirming its amorphous nature [J. Yan, 2014]. For GO, a new characteristic carbon peak (0 0 1) at $2\theta = 10.15^\circ$ with d = 0.87 nm (graph c) was observed due to an increase in the interlayer spacing of graphite. During oxidation of graphite into GO, inclusion of oxygen functionalities groups results in increasing the interlayer spacing between the graphene sheets [F.M. Casallas Caicedo, 2020]. The diffractogram of Q-rGO (graph d) showed the disappearance of GO peak at 10.15° and appearance of new peak (0 0 2) at 25.28° with d = 0.35 nm. The d space value of Q-rGO (d = 0.35 nm) was lesser when compared with the d space value of GO (d = 0.87 nm) and it is closely associated with the d space value of graphite (d = 0.33), this may be due to the re-establishment of sp2 carbon network, decrease in the oxygen groups and intercalated of quercetin during reduction [V. Sharma, 2017].

The UV–Vis absorption spectra were performed for the samples GO, Quercetin and Q-rGO in the aqueous medium (Fig. 1(ii)). The spectrum (a) showed major peaks at 368 nm and 254 nm corresponding to the cinnamoyl and benzoyl groups of a free form of quercetin [S.B. Bukhari, 2009]. In the spectrum (b) of GO, a peak at 233 nm and a shoulder peak at 309 nm corresponding to the $\pi-\pi^*$ transition of C═C and $n-\pi^*$ transition of C═O was observed, which indicates the oxidation of graphite [Z. Luo, 2009]. The spectrum of Q-rGO (c) showed a shift in the peak from 233 nm (π- π^* transition) to 266 nm due to the reduction of GO to Q-rGO and restoration of carbon conjugated structure [S. Yang, 2012]. A shoulder peak at 368 nm accompanied with rGO peak confirms the presence of quercetin along with rGO. The digital image of GO and Q-rGO suspension is shown as an inset Fig. 1(ii), where brown color GO suspension had turned into black color after reducing with quercetin.

The surface functional group of graphite electrodes before and after modifying with GO, quercetin and Q-rGO were characterized by ATR-IR spectrophotometer (Fig. 1 (iii). For paraffin wax impregnated graphite (PIG) electrode, the spectrum does not show any significant peak due to the absence of any functional groups. But for quercetin electrode, the spectra showed multiple peaks at 1670 cm^{-1} (C═O) 1317 cm^{-1} (C–H–O), 1558 cm^{-1} (C═C), 1260 cm^{-1} (C–O–C), 3412–2343 cm^{-1} (O–H) [T. Kumar, 2020]. The spectrum for GO showed a stretching vibration peak for the alkoxy group (C–O) at 1036 cm^{-1}, and the epoxy group (C–O) at 1224 cm^{-1}. Also, a peak at 1420 cm^{-1} (-OH) corresponding to the alcohol group was observed [B. Chandu, 2017]. The Q-rGO electrodes showed no distinct peaks for IR absorption but a characteristic peak for reduced carbon was observed at 1575 cm^{-1}. The IR fingerprint region of quercetin disappeared or a decrease in the peak intensity was observed during the reduction process.

Raman spectroscopy is considered as a promising technique for the characterization of carbon materials. The structure and quality of the carbon material can be analyzed precisely, as this technique gives information about the first-order scattering of sp^2 carbon atoms (G band) and breathing mode of κ-point photons of A_{1g} symmetry (D band) which are highly specific for graphitic materials. [S. Gurunathan, 2013]. Raman spectra for unmodified PIG, GO and Q-rGO electrodes were shown in Fig. 1 (iv). The G band for the unmodified PIG electrode appeared at 1564 cm^{-1} with the absence of the D band which indicates that the unmodified PIG electrode has no defect or there is no structural imperfection. For GO electrode, the Raman spectrum exhibited the G and D bands at 1584 cm^{-1} and 1344 cm^{-1}, respectively with a more intense D band when compared with the G band. Peak shift in the G band

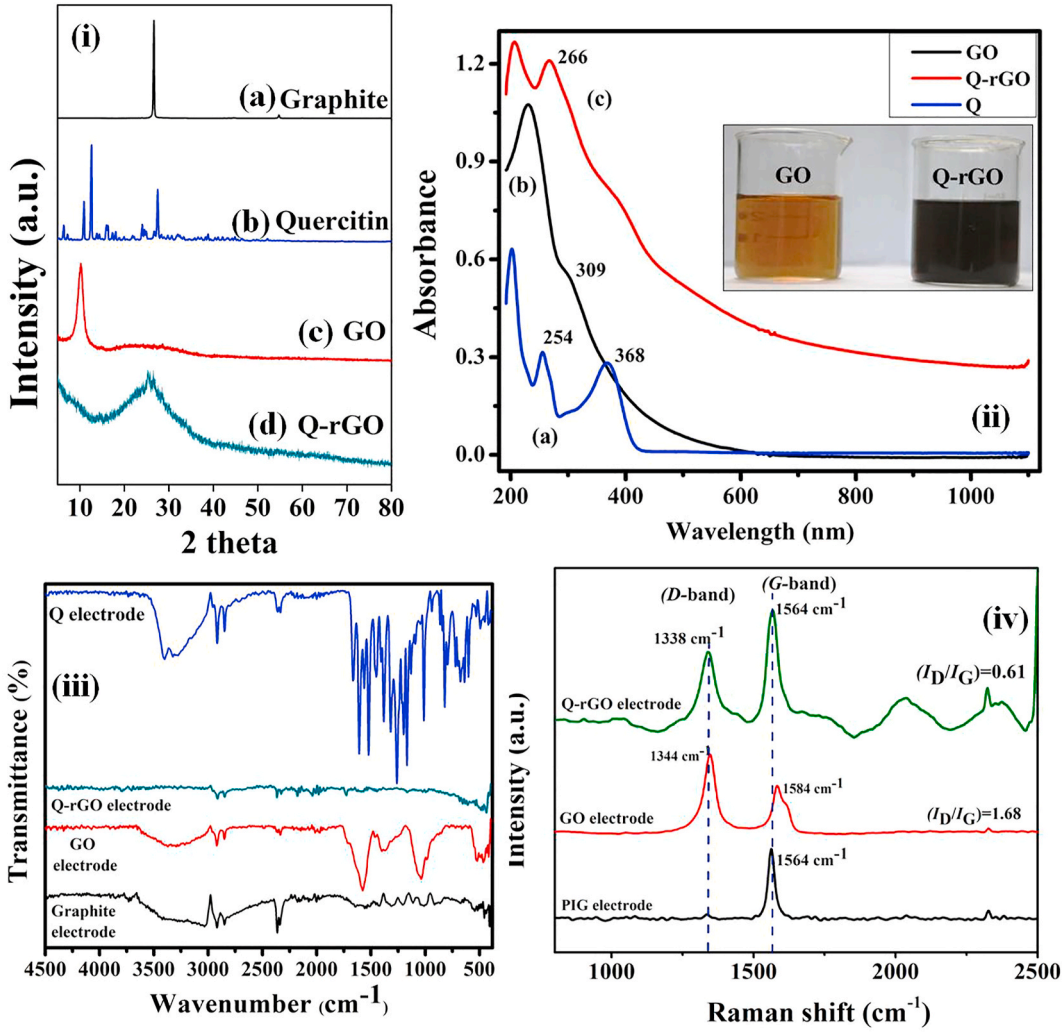

Figure-1. (i) XRD diffractrogram for (a) Graphite powder, (b) GO, and (c) Q-rGO, (ii) UV–Visible absorption spectra for (a) quercetin, (b) GO, and (c) Q-rGO, (iii) ATR-FTIR spectra and (iv) Raman spectra for the (black line) graphite electrode, (red line) GO electrode, (blue line) Quercetin (Q) electrode, (green line) Q-rGO electrode. (For interpretation of the references to color in this figure legend, the reader is referred to the Web version of this article.)

and increase in the intensity of D band shows higher defects, with the ratio of I_D/I_G for GO electrode as 1.68. This is due to the insertion of oxygen atom containing epoxide or hydroxyl group during the oxidation process of GO. As expected for the Q-rGO electrode, the Raman spectrum showed that the G band was shifted to its original position at 1564 cm^{-1} and the D band appeared to have less intensity with a shift in the peak at 1338 cm^{-1}. Comparatively the I_D/I_G ratio of Q-rGO was reduced to 0.61. The variation of intensity and peak position of both G and D band before and after the oxidation-reduction process was due to changes in the state of the electronic configuration of carbon [F.M. Casallas Caicedo, 2020].

3.2. Microscopic characterization

For HR-TEM analysis, the Q-rGO samples were dispersed in distilled water and sonicated until a homogenous suspension was obtained, the resulting suspension was coated onto a copper grid, air-dried and observed under HR-TEM. The microscopic image of Q-rGO showed a single sheet structure of exfoliated reduced graphene functionalized with quercetin which was highlighted in Fig. 2 (i) (a). The thickness of the Q-rGO 2D membrane was expected to be very less, approximately 10 nm due to the exfoliation of graphene and the reduction process. Fig. 2 (i) (b) is the higher magnification HR-TEM image of Q-rGO at the selected area, which showed discontinued fringes with the interlayer distance of 0.7–0.9 nm. The SAED pattern at selected area showed polycrystalline ring pattern with many diffraction spots (Fig. 2 (i) (c)) [F.M. Casallas Caicedo, 2020]. This result suggested that, the rGO sheets showed destruction of long-range ordering.

The surface morphology of unmodified PIG electrode, GO, quercetin, and Q-rGO electrodes were observed using FESEM. Fig. 2 (ii) shows the FESEM image of the unmodified PIG electrode (image a), where the surface seems to be clean and smooth. In GO electrode, (image b) showed multi-layered wrinkled carbon sheets present on the GO coated electrode surface. The FESEM of quercetin coated PIG electrode showing a cluster of spherical shaped agglomerated particles around 25 nm in size (image c). Exfoliation of graphene layer was observed in FESEM (image d) and functionalization of quercetin between the graphene layers was observed in the higher magnified image (e). The Q-rGO electrode with a wrinkled paper-like structure of monolayer rGO sheets was observed. The higher magnification of monolayered Q-rGO sheets and functionalization of the cluster of spherical nanoparticles revealed the presence of quercetin between the graphene layers.

3.3. Electrochemical characterization

The electrochemical behavior of unmodified PIG and different CMEs were studied using CV and EIS techniques. Fig. 3 (i) showed the CV curve for (a) unmodified PIG, (b) GO, (c) quercetin and (d) Q-rGO electrodes in blank 0.1 M KNO_3, at 50 mVs^{-1} scan rate. The unmodified

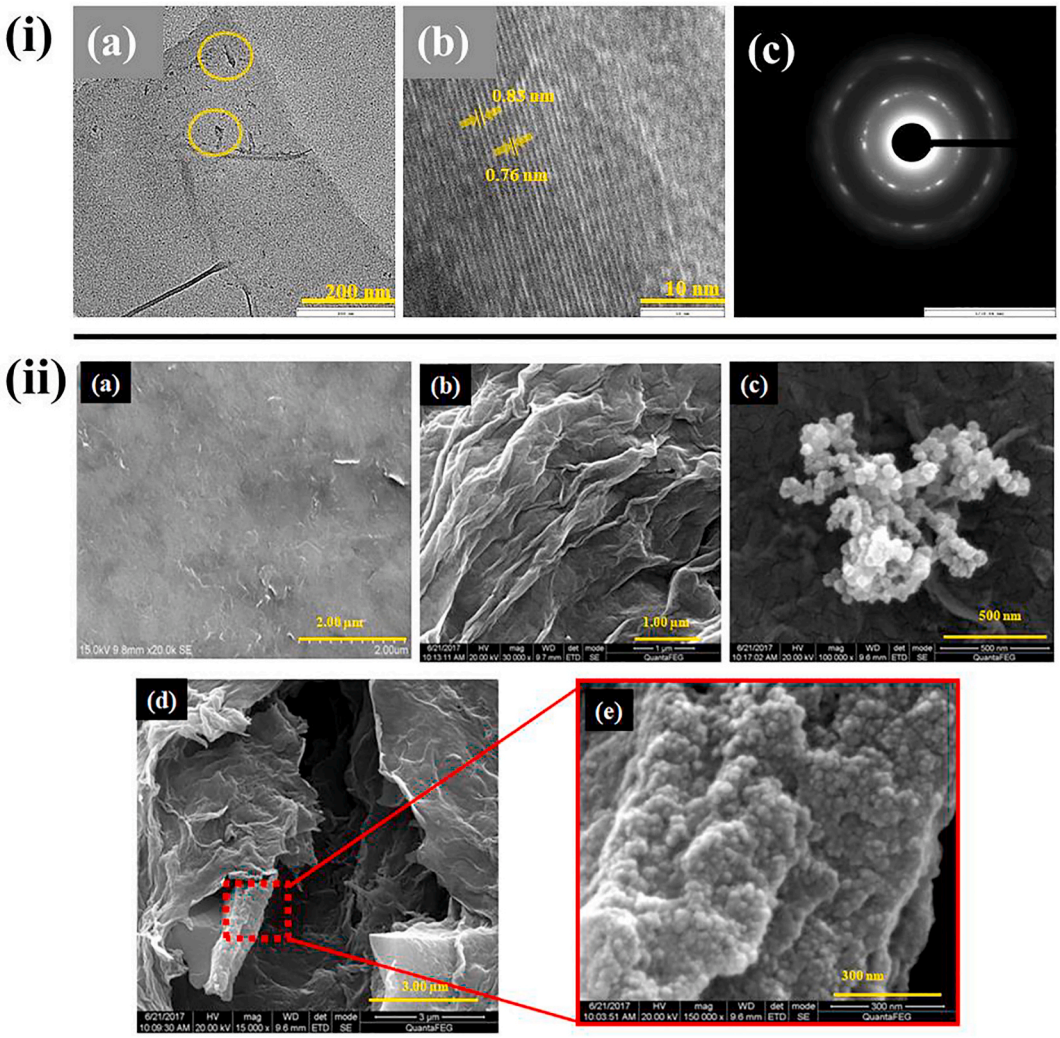

Fig. 2. (i) HR-TEM image of (a–b) Q-rGO, (c) SAED pattern; (ii) FESEM image of (a) unmodified PIG, (b) GO, (c) Quercetin, (d–e) Q-rGO electrodes.

PIG and GO electrodes (a & b) exhibit a plain CV curve without any redox behavior, but a change in the background current was observed. Naturally GO is considered to be a poor conductor [S. Stankovich, 2006], so the background current for the GO electrode is less compared to other modified electrodes. The CV curve c of quercetin electrode showed a redox peak at $Ep_a = 0.4$ V and $Ep_c = 0.28$ V. In Q-rGO electrode (curve d) a redox peak at $Ep_a = 0.5$ V, $Ep_c = 0.35$ V was observed. Compared with the quercetin electrode the intensity of background current for the Q-rGO electrode was found to be higher.

Herein, the electrochemical behavior of the unmodified PIG and different CMEs in 0.1 M KNO_3 electrolyte containing 1.0 mM of ($[Fe(CN)_6]^{3\ -/4}$) redox probe which was tested using CV technique. The Fig. 3 (ii) shows the CV curve for (a) unmodified PIG, (b) GO, and (c) Q-rGO electrodes in 0.1 M KNO_3 containing $[Fe(CN)_6]^{3\ -/4\ -}$ at the scan rate of 50 mVs^{-1}. The CV curve a for unmodified PIG electrode exhibited a redox peak at $Ep_a = 0.24$ V, and $Ep_c = 0.10$ V, respectively which corresponds to the redox process of Fe^{3+}/Fe^{2+}. A very low intensity redox peak at the same potential was observed for the GO electrode which was due to the poor electrical conductivity of GO (curve b). But for the Q-rGO electrode, there was an appearance of two anodic peaks $Ep_{a1} = 0.27$ V for oxidation of Fe^{2+}, $Ep_{a2} = 0.5$ V for oxidation of quercetin and two cathodic peaks $Ep_{c1} = 0.08$ V for reduction of Fe^{3+} and $Ep_{c2} = 0.41$ V for reduction of quercetin were observed. This proves that the electrochemical behavior of quercetin was enhanced upon functionalization with rGO.

Under the same electrolyte condition, the EIS analyses for all these electrodes were recorded (frequency range-100 to 0.01 kHz). The Fig. 3 (iii) shows the EIS plot for (a) unmodified PIG, (b) GO, (c) quercetin, and (d) Q-rGO electrodes. Each electrodes at higher frequency region showing the Nyquist plot containing semicircle due to the charge transfer resistance (R_{CT}) (inset figure) and linear part due to diffusion process at lower frequency region. From the inset Fig. 3 (iii), it was determined that the semicircle formed for quercetin was higher compared with unmodified PIG, and Q-rGO electrodes. This is due to the repulsion of charge creating resistance between quercetin and $[Fe(CN)_6]^{3-/4-}$ present in the electrolyte [Y. Yao, 2016]. The EIS plot for the GO electrode showed control of the diffusion process, as the linear part increased in the lower frequency. The GO electrode showed larger impedance and higher R_{CT} than other electrodes. Compared with the quercitin electrode the semicircle of the Q-rGO electrode was smaller which implies that the R_{CT} of Q-rGO is lesser. The impedance of Q-rGO electrode was less when compared to the quercetin and GO electrodes, whereas the unmodified PIG electrode showed higher impedance. Here the Q-rGO electrode showed an increased linear slop line exhibiting excellent capacitance behavior at a lower frequency [E. Casero, 2012]. This is evidence that Q-rGO film is capable of increasing the electron transfer process. A synergetic effect between Q and rGO could facilitate better electron transfer between electrode surface and electrolyte when compared with all other electrodes [Z. Wang, 2011]. Fig. 3 (iv) shows the Nyquist plot before and after fitting the derived equivalent circuit for

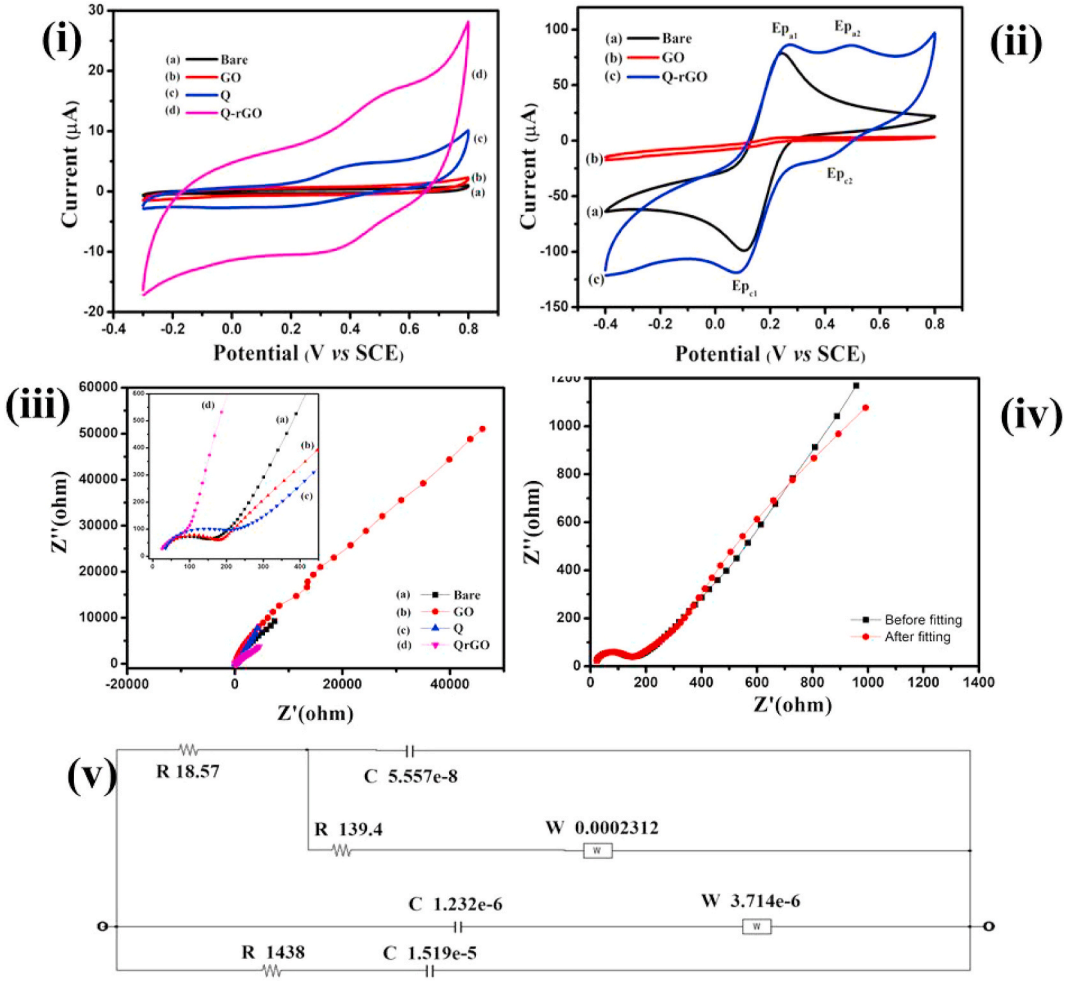

Fig. 3. (i) Cyclic voltammogram for (a) unmodified PIG, (b) GO, (c) Q and (d) Q-rGO electrodes in 0.1 M KNO_3 solution. (ii) Cyclic voltammogram for (a) unmodified PIG, (b) GO, and (c) Q-rGO electrodes in 0.1 M KNO_3 solution containing 1 mM of $K_3Fe(CN)_6$. Potential Scan −0.4 to +0.8 V at scan rate 50 mVs^{-1}. (iii) EIS plot for (a) unmodified PIG, (b) GO, (c) Q and (d) Q-rGO electrodes. (iv) EIS plot for Q-rGO electrode before and after fitting the equivalent circuit. (v) Corresponding equivalent circuit for Q-rGO electrode in 0.1 M KNO_3 solution containing 1 mM of $K_3Fe(CN)_6$.

the Q-rGO electrode. Based on the EIS graph for the Q-rGO electrode, an arbitrary equivalent circuit with complex elements was plotted (Fig. 3 (v)). An equivalent circuit derived from the Nyquist plot having a phase angle of 45°. The slope value account for the Warburg resistance (Z) followed by a large linear slope at lower frequency region accounts for the double layer capacitance (C) of Q-rGO electrodes was observed. Initially, there was a resistance created between working and reference electrode, and electrolyte interface. From the experimental results, we conclude that on comparing the R_{CT} obtained for unmodified PIG and Q-rGO electrodes, the R_{CT} for GO electrode is much higher.

3.4. Parameter optimization

Factors influencing the performance of the Q-rGO electrode during stripping analysis of metal ions were studied under different experimental conditions. The effect of background electrolyte, electrolyte pH and preconcentration time, were optimized for a fixed concentration of Cd (II) and Pb (II) ions.

The composition of background electrolyte may affect the complex formation of metal ions (Cd (II) and Pb (II)) at the active surface of the Q-rGO electrode. Hence experiments with different background electrolytes of fixed concentration (0.1 M) were studied. Chloride-based electrolytes (complexing anion) were avoided due to the precipitation of Pb (II) ions [H.C.H. Hahne, 1973], whereas nitrate and acetate (non--complexing anion) did not precipitate Pb (II) ions. Anodic stripping scans were performed from −1.0 to 0 V in different stripping medium such as (a) ammonium nitrate, (b) potassium nitrate, (c) sodium nitrate, (d) phosphate buffer, (e) acetate buffer, (f) potassium sulfate, (g) sodium sulfate and (h) ammonium sulfate. Fig. 4 (i) shows the bar chart representing the stripping current corresponding to Cd (II) and Pb (II) from Q-rGO electrodes in different electrolytes. Among all electrolytes, 0.1 M acetate buffer showed a better response with the maximum stripping signal for both the metal ions. Hence, the background electrolyte was choosen to be 0.1 M acetate buffer for further analysis.

The effect of pH plays an important role in the coordination of metals ions with Q-rGO electrode. The electrostatic attraction and repulsion of Cd (II) and Pb (II) ions depend on the surface charge density on the electrode [M. Grätzel, 2001]. The coordination of Cd (II) and Pb (II) with Q-rGO at the electrode surface was highly favoured in acidic medium whereas in the basic medium, metal/Q-rGO complex was less stable and may leach out from the electrode. Hence the pH of the acidic acetate buffer was chosen between 3.0 and 5.5 for further optimization. Fig. 4 (ii) shows the current response obtained during DPASV analysis for Cd (II) and Pb (II) preconcentrated Q-rGO electrodes in 0.1 M acidic acetate buffer with varying pH. The maximum response was obtained at pH 4.5. At pH > 4.5, hydrolysis of Pb (II) occurred which was not favourable for the coordination of metal ion with the modified electrode and hence a decrease in stripping signal was observed [S. Morante-Zarcero, 2010]. The same condition was found to be suitable for the stripping measurement of Cd (II) and maximum stripping current for both the metal

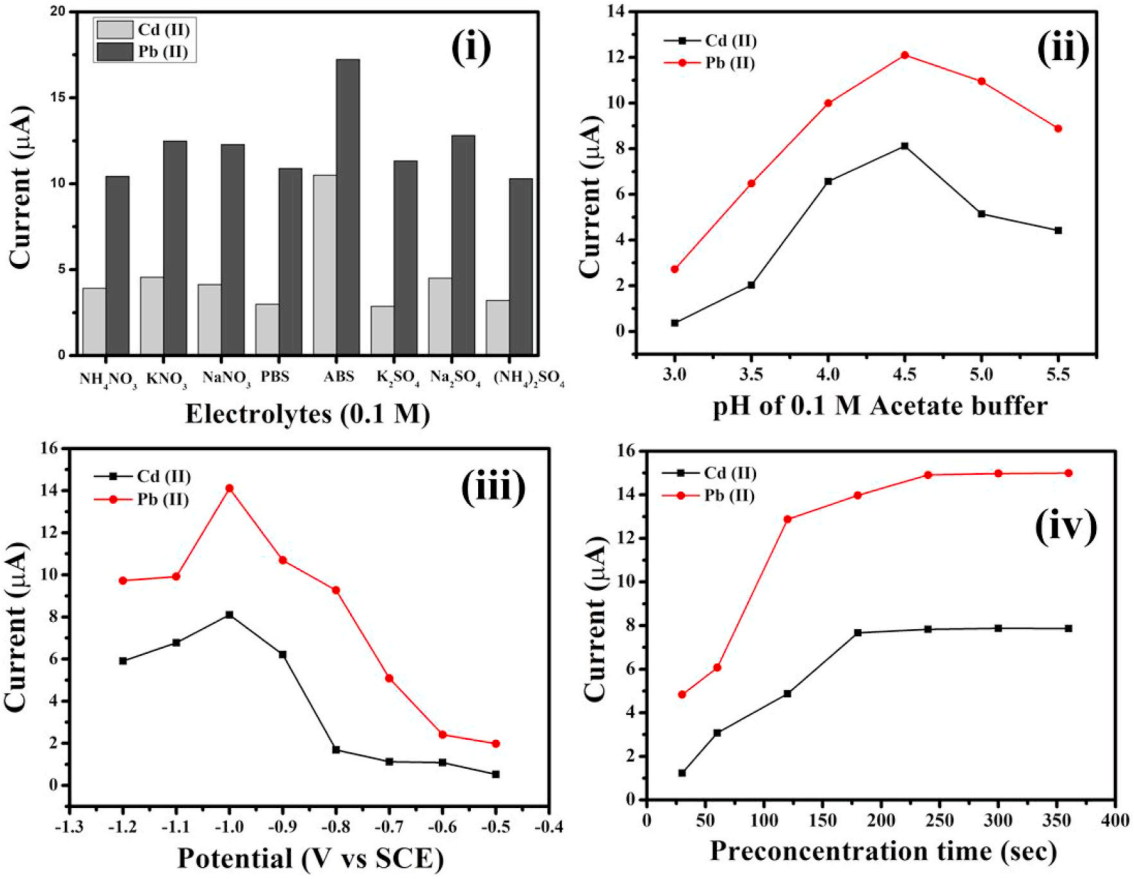

Fig. 4. The graph plot obtained from the current response during DPASV analysis of Cd (II) and Pb (II) ions by Q-rGO electrode under various experimental conditions (i) 0.1 M of different background electrolyte, (ii) pH effect, (iii) deposition potential and (iv) preconcentration time.

ions intensified under this condition. Therefore pH 4.5 was chosen for further analysis.

The metal ions were preconcentration from buffer solution to the surface of Q-rGO electrode, followed by reduction of Cd(II)-Q-rGO, Pb (II)-Q-rGO ions into Cd (0)-Q-rGO and Pb(0)-Q-rGO which was perfromed using chronoamperometry technique. By varying the potential from −0.4 to −1.2 V, the reduction of metal ions on the surface of the Q-rGO electrode was measured. The graph in Fig. 4. (iii) showed that the reduction potential range from −0.4 V till −0.6 V does not show significant difference in the stripping current, which means at these potentials the surface adsorption and reduction of Cd (II) and Pb (II) ions were poor. But further increase in the reduction potential beyond −0.7 V, there was a gradual increase in the stripping signal for Pb (II) and from −0.9 V for Cd (II) ions, respectively. Maximum stripping current was observed when the reduction potential of −1.0 V was applied for both the metal ions. Further increase in the reduction potential till −1.2 V, there was a decrease in the current intensity, this was due to evaluation of bubble at the modified electrode surface. When more negative potential was applied, the evaluation of bubble could inhibit the surface adsorbtion of metal ions over the Q-rGO electrode. Therefore the reduction potential was fixed as −1.0 V for both the metal ions.

The maximum time obtained by Q-rGO electrode to form complexation with Cd (II) and Pb (II) ions present in 0.1 M acetate buffer pH-4.5 was optimized by subjecting the modified electrode to the metal ion electrolyte solution for 30–360 s. Then the electrodes were washed, transferred to fresh electrolyte and DPASV response was recorded. From the graph plot results shown in Fig. 4 (iv), the DPASV response for the electrodes preconcentrated at the time interval from 30 to 240 s shows a steady increase in stripping current for Pb (II) and Cd (II). Preconcentration of Cd (II) ions over Q-rGO electrode attains saturation after 180 s, but for Pb (II), it is further extended to 240 s. The graph plot obtained from stripping current confirmed that the maximum intensity was obtained at 300 s, where the Q-rGO modified electrode attained saturation towards preconcentration Pb (II) and Cd (II) ions. Thus the duration of 300 s was choosen to be the optimal preconcentration time for the simultaneous analysis.

3.5. Electrochemical analysis

The DPASV analysis for Cd (II) and Pb (II) ions were determined individually using Q-rGO electrode with subsequent additions of both the metal ions into the optimized electrolyte condition. By applying a deposition potential of −1.0 V for a preconcentration time of about 300 s, the metal ions were reduced on the electrode surface. Fig. 5 (i) and (ii) shows the stripping voltammogram obtained for different concentration of Pb (II) and Cd (II) ion, respectively. As the figure showed that there was a gradual increase in the stripping peak current with good linearity as the concentration of metal ion increased in the electrolyte solution. The inset Fig. 5 (i) and (ii) showed the calibration plot for the concentration range from 0.19 to 3.1 μgL^{-1} ($R^2 = 0.9954$) for the Pb (II) ion and 0.19 to 2.5 μgL^{-1} ($R^2 = 0.9971$) for Cd (II) ions. The base current for the Q-rGO electrode in the blank electrolyte was measured for 10 times to obtain the standard deviation (SD). The limit of detection (LOD) was calculated using the equation, LOD = 3(SD)/slope, and limit of quantification (LOQ) was measured using the equation, LOQ = 10(SD)/slope. From the given equation, the LOD and LOQ for Pb (II) ion was found to be 0.06 μgL^{-1} and 0.21 μgL^{-1} respectively, LOD and LOQ for Cd (II) ion was found to be 0.05 μgL^{-1} and 0.184 μgL^{-1}, respectively.

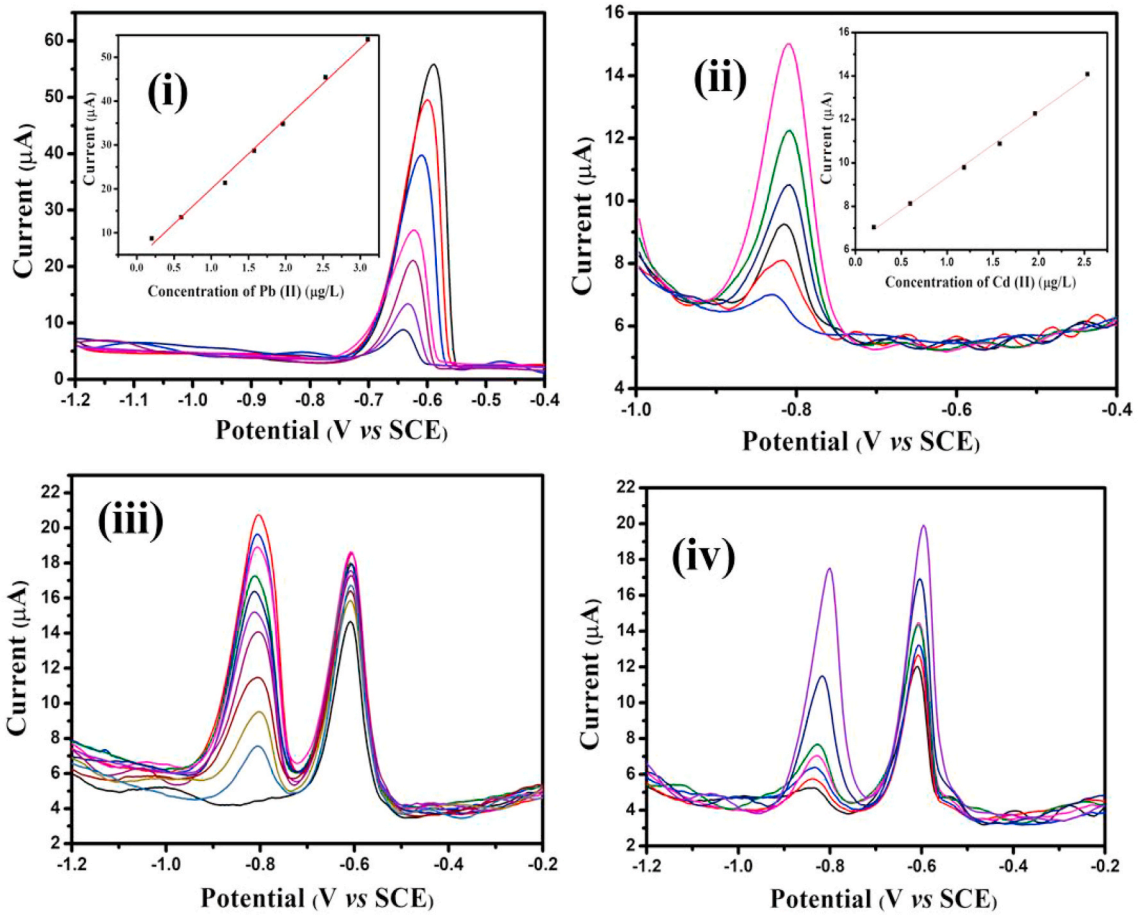

Fig. 5. DPASV curves of Q-rGO electrode for individual analysis of (i) Pb (II) and (ii) Cd (II) ions. (Inset) corresponding linear graphs. (iii) DPASV curves for different concentration of Cd (II) ions in the presence of Pb (II) ions. (iv) Simultaneous analysis of Cd (II) and Pb (II) ions. Background electrolyte, 0.1 M acetate buffer (pH-4.5), reduction potential-(-1.0 V), and preconcentration time-300 s.

3.6. Simultaneous analysis of Cd (II) and Pb (II) ions

Under optimized condition, Q-rGO electrode able to measure the Pb (II) ions even in the presence of Cd (II) ions. The stripping peak potential of Pb (II) ion was obtained at −0.58 V, showing a gradual increase in the intensity of peak current for every successive addition. During this process, a constant current was obtained for Cd (II) ions (figure not shown). The DPASV analysis was also performed to evaluate the influence of Pb (II) ions during the successive addition of Cd (II) ions. The stripping peak potential of Cd (II) ion was obtained at −0.8 V. The successive addition of Cd (II) ion showed an increase in the peak intensity and a slight variation in peak intensity of Pb (II) ions was observed (Fig. 5 (iii). This is because Cd (0) exhibited higher negative potential (−0.8 V) for the oxidation when compared with Pb (0), which in turn reflected at the oxidation potential of Pb (II) ions (−0.59 V). Also, the active site of the Q-rGO electrode was occupied preferentially by Pb (II) ions [37]. Fig. 5 (iv) showed the DPASV of simultaneous analysis of Pb (II) and Cd (II) ions, where an increase in the concentration of both the metal ions showed a gradual increase in both the peak current. The co-existence of both the peaks at −0.59 V and −0.8 V increased as the concentration of Pb (II) and Cd (II) ions increased from 0.19 to 2.5 μgL^{-1}. This was slightly different from the values obtained for the individual analysis. Interference of coexisting species was considered to be a common issue during simultaneous analysis. Therefore, the experiments were repeated five times and the reproducibility in the results was confirmed with the obtained relative standard deviation which is equal to 3.5%.

4. Conclusion

The present work described an ecofriendly approach towards synthesis of rGO and determination of Cd (II) and Pb (II) ions using DPASV technique. Toxic agents were avoided during the reduction of GO into rGO. During the synthesis of rGO, quercetin a natural flavonoid was used as a reducing and functionalizing agent. Presence of quercetin over rGO decreased the regraphitization property, thus retaining the electrical property of rGO. The physic-chemical characterization revealed that the material Q-rGO showed good electrical conductivity and metal complexing ability. The sensitivity of the quercetin was enhanced upon functionalizing with rGO. Further modifying the Q-rGO on PIG electrode surface which act as an alternate to mercury-free electrode for electrochemical sensing of metal ions. Under optimized condition, the Q-rGO electrode was capable of sensing Cd (II) and PB (II) ions individually and simultaneously. Even though quercetin-rGO has the property to form complex with some of the additional toxic metal ions, the optimized parameter such as selection of electrolyte, pH and preconcentration potential and time are more suitable for the selective determination of Cd (II) and Pb (II) ions. Parameters provided the analytical conditions where 0.1 M acetate buffer (pH-4.5) electrolyte, with the deposition potential of −1.0 V and preconcentration time of 300 s making it more suitable for Q-rGO electrode for effective sensing of Cd (II) and Pb (II) ions. Interference study showed that the 100 fold increase in the concentration of other metal ions does not alter the analytical results of Cd (II) ion and Pb (II) ion. The optimized condition provided suitable environment for the rapid sensing of both the metal ions without interference. Thus, the developed analytical method provided by green

chemistry approach which created a new dimension in the synthesis of rGO and simultaneous sensing of metal ions in the concentration of Cd (II) ion form 0.19 to 2.5 μgL^{-1} with LOD-0.05 μgL^{-1} and Pb (II) ions from 0.19 to 3.1 μgL^{-1} with LOD 0.06 μgL^{-1}, respectively.

Credit author statement

K. Krishna Kumar: Investigation, Methodology and Writing - Original Draft. M. Devendiran: Investigation, Methodology; Formal analysis. P. Senthil Kumar*: Conceptualization, Validation and Supervision. S. Sriman Narayanan: Conceptualization, Validation and Supervision

Declaration of competing interest

The authors declare that they have no known competing financial interests or personal relationships that could have appeared to influence the work reported in this paper.

References

Hassan, Karimi-Maleh, Lütfi Yola, Mehmet, Atar, Necip, YasinOrooji, Fatemeh Karimi, Senthil Kumar, P., Rouhi, Jalal, Baghayeri, Mehdi, 2021. A novel detection method for organophosphorus insecticide fenamiphos: molecularly imprinted electrochemical sensor based on core-shell Co_3O_4@MOF-74 nanocomposite. J. Colloid Interface Sci. 592, 174–185.

Akin, I., Zor, E., Bingol, H., Ersoz, M., 2014. Green synthesis of reduced graphene oxide/polyaniline composite and its application for salt rejection by polysulfone-based composite membranes. J. Phys. Chem. B 118, 5707–5716.

Anitha, T., Kumar, P.S., Kumar, K.S., Ramkumar, B., Ramalingam, S., 2015. Adsorptive removal of Pb(II) ions from polluted water by newly synthesized chitosan–polyacrylonitrile blend: equilibrium, kinetic, mechanism and thermodynamic approach. Process Saf. Environ. Protect. 98, 187–197.

Aunkor, M.T.H., Mahbubul, I.M., Saidur, R., Metselaar, H.S.C., 2016. The green reduction of graphene oxide. R.S.C. Adv, RSC Advances 27807–27828.

Balandin, A.A., Ghosh, S., Bao, W., Calizo, I., Teweldebrhan, D., Miao, F., Lau, C.N., 2008. Superior thermal conductivity of single-layer graphene. Nano Lett. 8 (3), 902–907.

Hassan, Karimi-Maleh, Alizadeh, Marzieh, Orooji, Yasin, Karimi, Fatemeh, Baghayeri, Mehdi, Rouhi, Jalal, Tajik, Somayeh, Beitollahi, Hadi, Agarwal, Shilpi, Gupta, Vinod K., Rajendran, Saravanan, Rostamnia, Sadegh, Fu, Li, Saberi-Movahed, Farshad, Malekmohammadi, Samira, 2021. Guanine-based dna biosensor amplified with Pt/SWCNTs nanocomposite as analytical tool for nanomolar determination of daunorubicin as an anticancer drug: a docking/experimental investigation. Ind. Eng. Chem. Res. 60 (2), 816–823.

Bo, Z., Shuai, X., Mao, S., Yang, H., Qian, J., Chen, J., Yan, J., Cen, K., 2014. Green preparation of reduced graphene oxide for sensing and energy storage applications. Sci. Rep. 4, 4684.

Bukhari, S.B., Memon, S., Mahroof-Tahir, M., Bhanger, M.I., 2009. Synthesis, characterization and antioxidant activity copper-quercetin complex. Spectrochim. Acta Part A Mol. Biomol. Spectrosc. 71, 1901–1906.

Casallas Caicedo, F.M., Vera López, E., Agarwal, A., Drozd, V., Durygin, A., Franco Hernandez, A., Wang, C., 2020. Synthesis of graphene oxide from graphite by ball milling. Diam. Relat. Mater. 109.

Casero, E., Parra-Alfambra, A.M., Petit-Domínguez, M.D., Pariente, F., Lorenzo, E., Alonso, C., 2012. Differentiation between graphene oxide and reduced graphene by electrochemical impedance spectroscopy (EIS). Electrochem. Commun. 20, 63–66.

Chandu, B., Mosali, V.S.S., Mullamuri, B., Bollikolla, H.B., 2017. A facile green reduction of graphene oxide using annona squamosa leaf extract. Carbon Lett 21, 74–80.

Devendiran, R.M., Chinnaiyan, S.K., Yadav, N.K., Ramanathan, G., Singaravelu, S., Perumal, P.T., Sivagnanam, U.T., 2016. Facile synthesis and evaluation of quercetin reduced and dextran sulphate stabilized gold nanoparticles decorated with folic acid for active targeting against breast cancer. RSC Adv. 6, 32560–32571.

Gadgil, B., Damlin, P., Kvarnström, C., Sc, 2016. Graphene vs. reduced graphene oxide: a comparative study of graphene-based nanoplatforms on electrochromic switching kinetics. Carbon N. Y. 96, 377–381.

Geim, A.K., Novoselov, K.S., 2007. The rise of graphene. Nat. Mater. 6, 183–191.

Gnana Kumar, G., Justice Babu, K., Nahm, K.S., Hwang, Y.J., 2014. A facile one-pot green synthesis of reduced graphene oxide and its composites for non-enzymatic hydrogen peroxide sensor applications. RSC Adv. 4, 7944–7951.

Grätzel, M., 2001. Photoelectrochemical cells. Nature 414, 338–344.

Gurunathan, S., Han, J.W., Kim, J.H., Humanin, 2013. A novel functional molecule for the green synthesis of graphene. Colloids Surf. B Biointerfaces 111, 376–383.

Hahne, H.C.H., Kroontje, W., 1973. Significance of pH and chloride concentration on behavior of heavy metal pollutants: mercury(II), cadmium(II), zinc(II), and lead(II)1. J. Environ. Qual. 2, 444.

HarshaVardhan, Kilaru, SenthilKumar, Ponnusamy, Panda, Rames C., 2019. A review on heavy metal pollution, toxicity and remedial measures: current trends and future perspectives. J. Mol. Liq. 290, 111197.

Hatamie, S., Akhavan, O., Sadrnezhaad, S.K., Ahadian, M.M., Shirolkar, M.M., Wang, H. Q., 2015. Curcumin-reduced graphene oxide sheets and their effects on human breast cancer cells. Mater. Sci. Eng. C 55, 482–489.

Hummers, William S., Offeman, Richard E., 1958. Preparation of graphitic oxide. J. Am. Chem. Soc. 80 (6), 1339.

Isai, K.A., Shrivastava, V.S., 2015. Detection and identification of organics and metals from industrial wastewater by ICP-aes, FTIR and GC-MS. Journal of Advanced Chemical Sciences 1 (4), 164–166.

Karimi-Maleh, Hassan, Karimi, Fatemeh, Orooji, Yasin, Mansouri, Ghobad, Razmjou, Amir, Aygun, Aysenur, Sen, Fatih, 2020. A new nickel-based co-crystal complex electrocatalyst amplifed by NiO dope Pt nanostructure hybrid; a highly sensitive approach for determination of cysteamine in the presence of serotonin. Sci. Rep. 10, 11699.

Kumar, T., Shrivas, K., Kurrey, R., Upadhyay, S., Jangde, R., Chauhan, R., 2020. Spectrochimica Acta Part A : molecular and Biomolecular Spectroscopy Phytochemical screening and determination of phenolics and fl avonoids in Dillenia pentagyna using UV – vis and FTIR spectroscopy. Spectrochim. Acta Part A Mol. Biomol. Spectrosc. 242, 118717.

Lee, C., Wei, X., Kysar, J.W., Hone, J., Lee, C., Wei, X., Kysar, J.W., Hone, J., 2016. Measurement of the elastic properties and intrinsic strength of monolayer, graphene. AAAS Science 321, 385–388.

Lu, Y., Liang, X., Niyungeko, C., Zhou, J., Xu, J., Tian, G., 2018. A review of the identification and detection of heavy metal ions in the environment by voltammetry. Talanta 178, 324–338.

Luo, Z., Lu, Y., Somers, L.A., Johnson, A.T.C., 2009. High Yield Preparation of Macroscopic Graphene Oxide Membranes, pp. 898–899.

Maddinedi, S.B., Mandal, B.K., 2016. Biofabrication of reduced graphene oxide nanosheets using Terminalia bellirica fruit extract. Curr. Nanosci. 12, 94–102.

Mohanraj, J., Durgalakshmi, D., Ajay Rakkesh, R., Balakumar, S., Rajendran, S., Karimi-Maleh, 2020. Facile synthesis of paper based graphene electrodes for point of care devices: a double stranded DNA (dsDNA) biosensor. J. Colloid Interface Sci. 566, 463–47.

Morante-Zarcero, S., Sánchez, A., Fajardo, M., del Hierro, I., Sierra, I., 2010. Voltammetric analysis of Pb(II) in natural waters using a carbon paste electrode modified with 5-mercapto-1-methyltetrazol grafted on hexagonal mesoporous silica. Microchim. Acta. 169, 57–64.

Novoselov, K.S., Geim, A.K., Morozov, S.V., Jiang, D., Zhang, Y., Dubonos, S.V., Grigorieva, I.V., Firsov, A.A., 2004. Electric field effect in atomically thin carbon films. Science 306, 666–669.

Novoselov, K.S., Two-dimensional atomic crystals, Jiang, DNovoselov, K.S., Jiang, D., Schedin, F., Booth, T.J., Khotkevich, V.V., Morozov, S.V., Geim, A.K., Schedin, F., Booth, T.J., V Khotkevich, V., V Morozov, S., Geim, A.K., 2005. Two-dimensional atomic crystals. Proc. Natl. Acad. Sci. Unit. States Am. 102, 10451–10453.

Rojas, C., Arancibia, V., Gómez, M., Nagles, E., 2013. High sensitivity adsorptive stripping voltammetric method for antimony(III) determination in the presence of quercetin-5′-sulfonic acid. Substituent effect on sensitivity. Sensor. Actuator. B Chem. 185, 560–567.

Saravanan, A., SenthilKumar, P., Yaashikaa, P.R., Karishma, S., Jeevanantham, S., Swetha, S., 2021a. Mixed biosorbent of agro waste and bacterial biomass for the separation of Pb(II) ions from water system. Chemosphere 227, 130236.

Saravanan, A., Senthil Kumar, P., Vo, Dai-Viet N., Swetha, S., Tsopbou Ngueagni, P., Karishma, S., Jeevanantham, S., Yaashikaa, P.R., 2021b. Ultrasonic assisted agro waste biomass for rapid removal of Cd(II) ions from aquatic environment: mechanism and modelling analysis. Chemosphere 271, 129484.

Sarzanini, C., Bruzzoniti, M.C., 2001. Metal species determination by ion chromatography. Trac. Trends Anal. Chem. 20 (6–7), 304–310.

Scholz, F., Lange, B., 1992. Abrasive stripping voltammetry - an electrochemical solid state spectroscopy of wide applicability. Trends Anal. Chem. 11, 359–367.

Sharma, V., Jain, Y., Kumari, M., Gupta, R., Sharma, S.K., Sachdev, K., 2017. Synthesis and characterization of graphene oxide (GO) and reduced graphene oxide (rGO) for gas sensing application. Macromol. Symp. 376.

Singh, C., Ali, M.A., Sumana, G., 2016. Green synthesis of graphene based biomaterial using fenugreek seeds for lipid detection. ACS Sustain. Chem. Eng. 4, 871–880.

Singhbabu, Y.N., Sahu, K.K., Dadhich, D., Pramanick, A.K., Mishra, T., Sahu, R.K., 2013. Capsule-embedded reduced graphene oxide: synthesis, mechanism and electrical properties. J. Mater. Chem. C. 1, 958–966.

Siraj, Khalid, Addisu Kitte, Shimeles, 2013. Analysis of copper, zinc and lead using atomic absorption spectrophotometer in ground water of jimma town of southwestern Ethiopia. International Journal of Chemical and Analytical Science 4 (Issue 4), 201–204.

Sriram, G., Bhat, M.P., Patil, P., Uthappa, U.T., Jung, H.Y., Altalhi, T., Kumeria, T., Aminabhavi, T.M., Pai, R.K., Kurkuri, M.D., 2017. Paper-based microfluidic analytical devices for colorimetric detection of toxic ions: a review. Trends Anal. Chem. 93, 212–227.

Stankovich, S., Dikin, D., Dommett, G., 2006. Graphene-based composite materials. Nature 442, 282–286.

Suganya, S., Senthil Kumar, P., 2018. Influence of ultrasonic waves on preparation of active carbon from coffee waste for the reclamation of effluents containing Cr(VI) ions. J. Ind. Eng. Chem. 60, 418–430.

Tahernejad-Javazmi, F., Shabani-Nooshabadi, M., Karimi-Maleh, H., 2018. Analysis of glutathione in the presence of acetaminophen and tyrosine via an amplified electrode with MgO/SWCNTs as a sensor in the hemolyzed erythrocyte. Talanta 176, 208–213.

Tahernejad-Javazmi, F., Shabani-Nooshabadi, M., Karimi-Maleh, H., 2019. 3D reduced graphene oxide/FeNi3-ionic liquid nanocomposite modified sensor; an electrical

synergic effect for development of tert-butylhydroquinone and folic acid sensor. Compos. B Eng. 172, 666–670.
Thakur, S., Karak, N., 2015. Alternative Methods and Nature-Based Reagents for the Reduction of Graphene Oxide - a Review. Carbon N. Y.
Wang, Y.F.X., Lu, D.M.S., 2014. Production of monolayer , trilayer , and multi-layer graphene sheets by a re-expansion and exfoliation method. J. Mater. Sci. 49, 2315–2323.
Wang, Y., Shi, Z.X., Yin, J., 2011a. Facile synthesis of soluble graphene via a green reduction of graphene oxide in tea solution and its biocomposites. ACS Appl. Mater. Interfaces 3, 1127–1133.
Wang, Z., Xia, J., Zhu, L., Chen, X., Zhang, F., Yao, S., Li, Y., Xia, Y., 2011b. A selective voltammetric method for detecting dopamine at quercetin modified electrode incorporating graphene. Electroanalysis 23, 2463–2471.
Yan, J., Wu, Y.H., Yu, D.G., Williams, G.R., Huang, S.M., Tao, W., Sun, J.Y., 2014. Electrospun acid-base pair solid dispersions of quercetin. RSC Adv. 4, 58265–58271.
Yang, S., Yue, W., Huang, D., Chen, C., Lin, H., Yang, X., 2012. A facile green strategy for rapid reduction of graphene oxide by metallic zinc. RSC Adv. 2, 8827–8832.
Yao, Y., Liu, Y., Yang, Z., 2016. A novel electrochemical sensor based on a glassy carbon electrode modified with Cu-MWCNT nanocomposites for determination of hydroquinone. Anal. Methods. 8, 2568–2575.
Zsembik, B.A., 2006. Health issues in latino families and households, Handb. Fam. Heal. Interdiscip. Perspect. 6, 40–61.